Strong ground motions from the 2010-2011 Canterbury earthquakes and the predictive capability of empirical and physics-based simulation models

B.A. Bradley, S. Jeong, H.N.T. Razafindrakoto

University of Canterbury, Christchurch, New Zealand

ABSTRACT: The 2010-2011 Canterbury earthquakes were recorded over a dense strong motion network in the near-source region, yielding significant observational evidence of seismic complexities, and a basis for interpretation of multi-disciplinary datasets and induced damage to the natural and built environment. This paper provides an overview of observed strong motions from these events and retrospective comparisons with both empirical and physics-based ground motion models. Both empirical and physics-based methods provide good predictions of observations at short vibration periods in an average sense. However, observed ground motion amplitudes at specific locations, such as Heathcote Valley, are seen to systematically depart from 'average' empirical predictions as a result of near surface stratigraphic and topographic features which are well modelled via site-specific response analyses. Significant insight into the long period bias in empirical predictions is obtained from the use of hybrid broadband ground motion simulation. The comparison of both empirical and physics-based simulations against a set of 10 events in the sequence clearly illustrate the potential for simulations to improve ground motion and site response prediction, both at present, and further in the future.

1   INTRODUCTION

The 2010-2011 Canterbury earthquake sequence includes the 4 September 2010 M_w7.1 Darfield earthquake (e.g. Gledhill et al. 2011) and three subsequent earthquakes of $M_w \geq 5.9$, most notably the 22 February 2011 M_w6.2 Christchurch earthquake (e.g. Bradley et al. 2014, Kaiser et al. 2012). The M_w6.2 Christchurch earthquake caused significant damage to commercial and residential buildings of various eras (Buchanan et al. 2011, Clifton et al. 2011, Kam et al. 2011). The severity and spatial extent of liquefaction observed in native soils was profound, and was the dominant cause of damage to residential houses, bridges and underground lifelines (Cubrinovski et al. 2011a). Rockfall and cliff collapse occurred in many parts of southern Christchurch (Dellow et al. 2011, Massey et al. 2014). The 13 June 2011 M_w6.0 earthquake caused further damage to previously damaged structures and severe liquefaction and rockfalls, and similarly for the M_w5.8 and M_w5.9 earthquakes on 23 December 2011. Several additional smaller aftershocks have also induced localized surface manifestations of liquefaction (e.g. Quigley et al. 2013), rockfall and building damage. This paper provides an overview of observed strong motions from these events and retrospective comparisons with both empirical and physics-based ground motion models.

2   OBSERVED GROUND MOTIONS

The 2010-2011 Canterbury earthquakes were recorded on a dense strong motion network maintained by GeoNet (www.geonet.org.nz) (Berrill et al. 2011). For illustration, Figure 1 displays the fault-normal acceleration time series recorded over the Canterbury region during the Darfield earthquake and over the Christchurch urban region during the Christchurch earthquake. The dense array of observed strong motions contain many amplitudes that had not previously been exceeded in New Zealand (principally due to a short observation period with the current GeoNet network), and a rich dataset for both examination of induced damage in the Canterbury earthquakes as well as a fundamental critique of the ability of empirical and physics-based ground motion models to predict such motions, which is elaborated upon in subsequent sections.
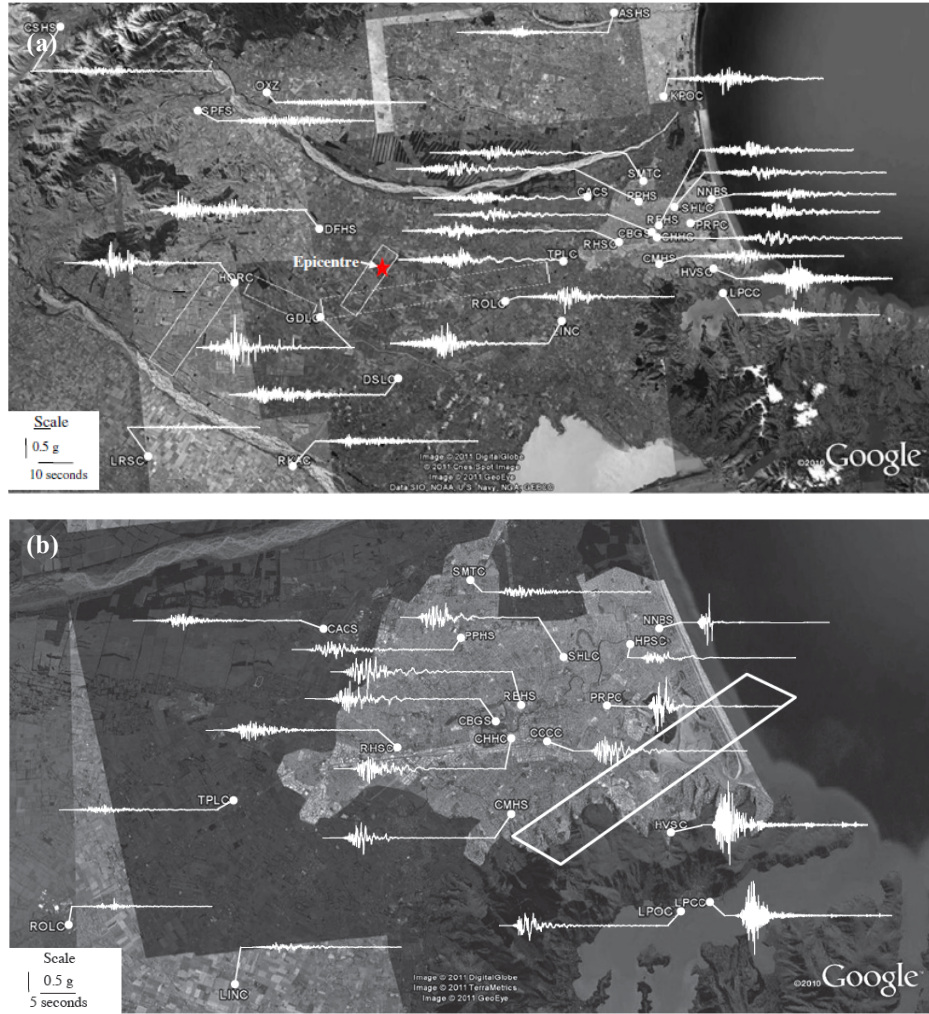
Figure 1: Fault normal acceleration time series recorded at strong motion stations in the Canterbury and Christchurch region during: (a) the 4 September 2010 Darfield earthquake; and (b) the 22 February 2011 Christchurch earthquake (after Bradley (2012b) and Bradley and Cubrinovski (2011)).

As documented extensively by others (Bray et al. 2014, Clifton et al. 2011, Kam et al. 2011), the damage to commercial structures in the Christchurch Central Business District (CBD) was severe, with current estimates that approximately 70% of all structures in the CBD have been, or will be, demolished (Marquis et al. 2015). Figure 2 illustrates the geometric mean horizontal response spectra recorded at the four strong motion stations within the Christchurch CBD during each of the four main earthquake events in the sequence. Despite their geographic separation distances (relative to their respective source-to-site distances), the characteristics of the ground motion observed at these locations are relatively similar. This is particularly the case for long-period ground motion ($T > 3$ s) amplitudes, which have longer wavelengths and therefore are expected to be more coherent. On the other hand, at short vibration periods there is a more pronounced difference in accelerations due to the ability of shorter wavelength energy to sample local heterogeneities in the crust, including the local nonlinear response of significantly different surficial soil layers (Cubrinovski et al. 2011b). During the 4 September 2010 Darfield earthquake, with the exception of Resthaven (REHS), ground motion amplitudes were generally below the design spectra for short-to-moderate periods (i.e. $T<2$s), and greater at $T=2$-3 seconds. For the 22 February 2011 Christchurch earthquake, ground motion amplitudes were greater than the 500 year design spectra at all vibration periods. The 13 June 2011 $M_w6.0$ event produced ground motions nearly equal to design spectral ordinates over a wide range of periods, while the 23 December 2011 $M_w5.9$ event produced significant spectral amplitudes primarily only at short-to-moderate vibration periods (with the exception of the REHS station).
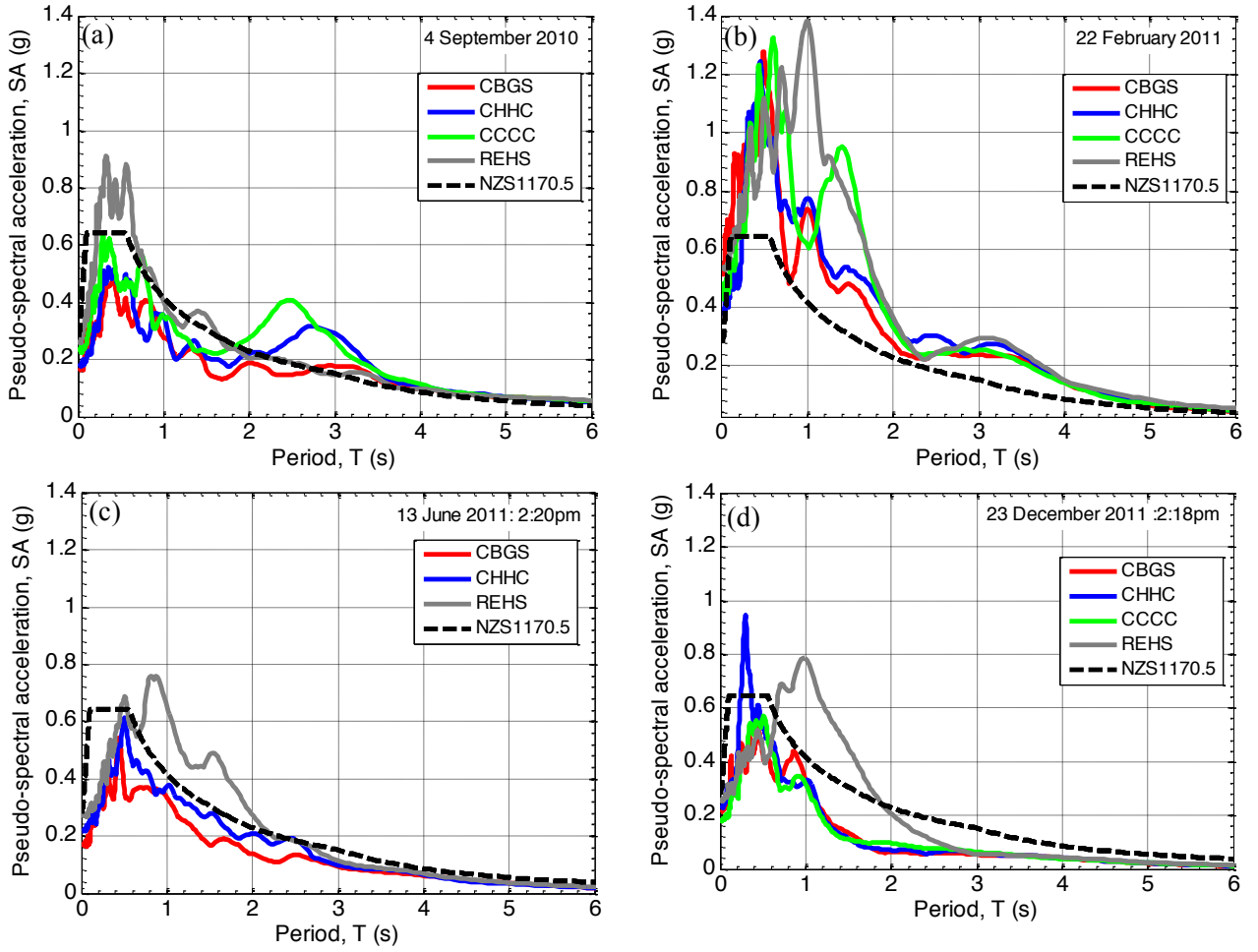
2

Figure 2. Geometric mean pseudo-spectral acceleration observed in the Christchurch CBD during the: (a) 4 September 2010 $M_w7.1$; (b) 22 February 2011 $M_w6.2$; (c) 13 June 2011 $M_w6.0$; (d) 23 December 2011 $M_w5.9$ Canterbury earthquakes. No recording at CCCC was obtained in the 13 June 2011 event (after Bradley et al. (2014)).

3 OBSERVATIONS VS PREDICTIONS FROM EMPIRICAL MODELS

3.1 *Comparison of response spectral ordinates*

The high quality and spatial density of the observed ground motions in the Canterbury earthquakes provide a unique opportunity to examine the predictive capabilities of empirical ground motion models, which are utilized for conventional seismic hazard analysis in New Zealand. Here attention is restricted to comparisons with the NZ-specific shallow crustal prediction model of Bradley (2013). More detailed comparisons can be found elsewhere (Bradley 2012b, Bradley 2013, Bradley and Cubrinovski 2011, Bradley et al. 2014). Figure 3 and Figure 4 illustrate the pseudo-acceleration response spectra (SA) amplitudes of ground motions at periods of $T = 0.0, 0.2, 1.0,$ and 3.0s recorded in the 4 September 2010 Darfield and 22 February 2011 Christchurch earthquakes, respectively. In order to emphasise strong ground-motion prediction, only ground motions within 100km and 50km from the causative faults in the Darfield and Christchurch earthquakes, respectively, are shown in the figures. The observations are compared with the NZ-specific SA model. For each of the different vibration periods considered, the median, 16th and 84th percentiles of the prediction for site class D conditions are shown. Mixed-effects regression was utilized in order to determine the inter- and intra-event results for each vibration period. The value of the normalized inter-event residual (η) is also shown in the inset of each figure.
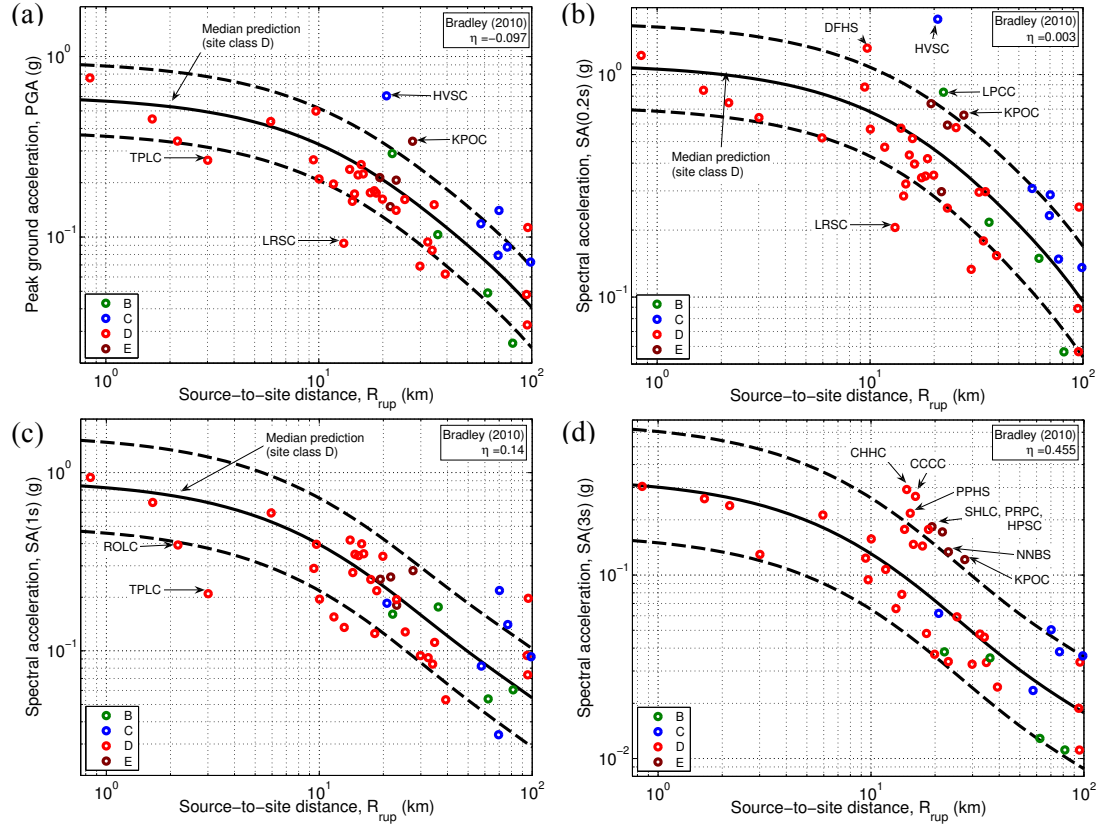
Figure 3: Pseudo-acceleration response spectral amplitudes observed in the 4 September 2010 Darfield earthquake in comparison with empirical prediction equations (after Bradley (2012b)).
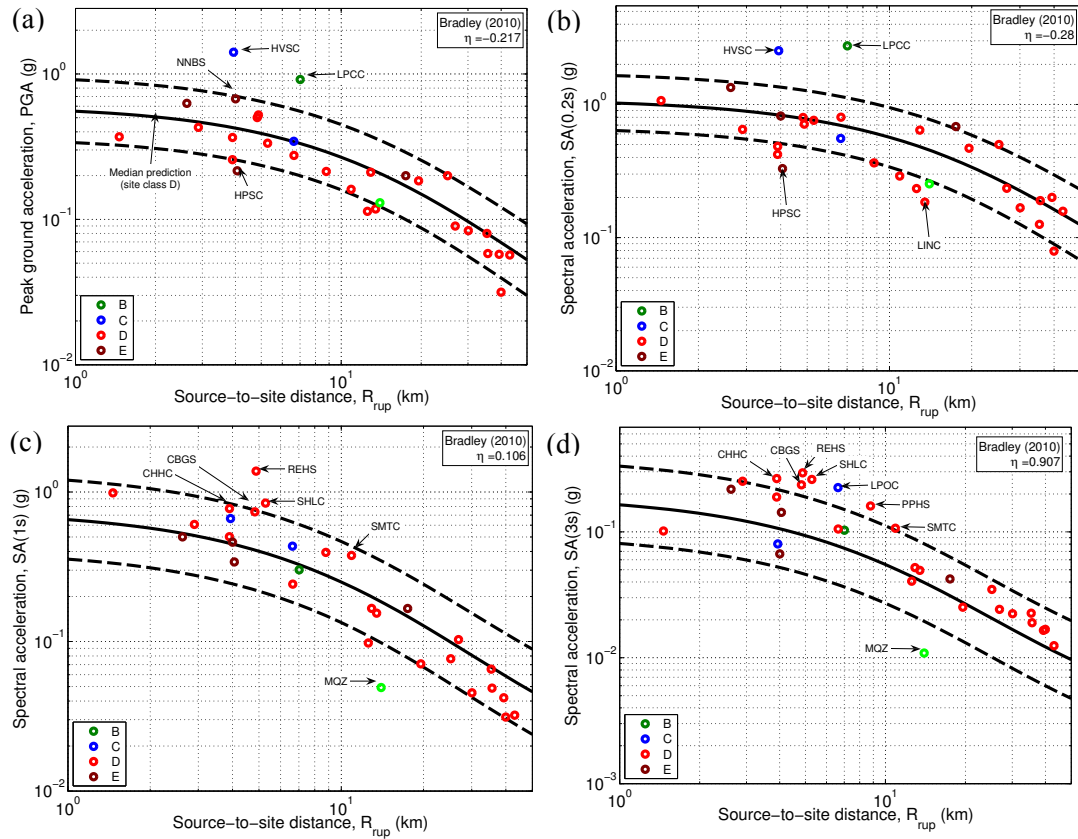

Figure 4: Comparison of pseudo-acceleration response spectral amplitudes observed in the 22 February 2011 Christchurch earthquake in comparison with empirical prediction equations (modified after Bradley (2013)).

The results of Figure 3 and Figure 4 illustrate that the NZ-specific empirical model is able to capture the source-to-site distance dependence of the observations with good accuracy. The inter-event term, which can be viewed as an overall bias of the amplitudes predicted relative to those observed, indicates that the model has very small bias for vibration periods of $T = 0.0, 0.2,$ and 1.0 s in both events. However, Figure 3d and Figure 4d illustrate that there is a notable under prediction of SA(3s) amplitudes in both the Darfield and Christchurch earthquakes (i.e. $\eta = 0.455$ and 0.907, respectively), the systematic nature of which is examined further in the next section.

3.2 *Systematic site effects via non-ergodic ground motion analysis*

As a result of a high density of strong motion instruments in the Canterbury region and the multiple events in the earthquake sequence, a significant number of high amplitude near-source ground motion have been recorded at the same location over these multiple events, as illustrated in Figure 5. Such a relatively unique ground motion dataset allows for the opportunity to directly examine systematic and repeatable ground motion phenomena. Such systematic effects have been qualitatively noted in the Canterbury ground motions (Bradley 2012a), but significant additional insight can be gained by quantitative analysis (Bradley 2015). In order to capture such systematic effects, the representation of SA, from event *e*, at a single site *s,* for the purposes of ground motion prediction, can be expressed as:

$$lnSA_{es} = f_{es}(Site, Rup) + (\delta L2L_l + \delta B_{el}^0) + (\delta S2S_s + \delta W_{es}^0) \qquad (1)$$

where $lnSA_{es}$ is the (natural) logarithm of the observed SA; $f_{es}(Site, Rup)$ is the median of the predicted logarithm of SA given by an empirical ground motion model, which is a function of the site and earthquake rupture considered; The first bracketed term is the between-event residual, $\delta B_e = (\delta L2L_l + \delta B_{el}^0)$, which can be expressed in the form of a systematic region-dependent factor, $\delta L2L_l$, and the remaining between-event residual, δB_{el}^0, for the given region that varies from event to event; The second bracketed term is the within-event residual, $\delta W_{es} = (\delta S2S_s + \delta W_{es}^0)$, which can be expressed in the form of a systematic site-dependent factor, $\delta S2S_s$, and a remaining within-event residual, δW_{es}^0, that varies from site-to-site and event-to-event. A summary of the systematic biases of observed ground motions in the Canterbury earthquakes is presented below for 10 earthquake events and 20 strong motion stations, further details of which can be found in Bradley (2015).
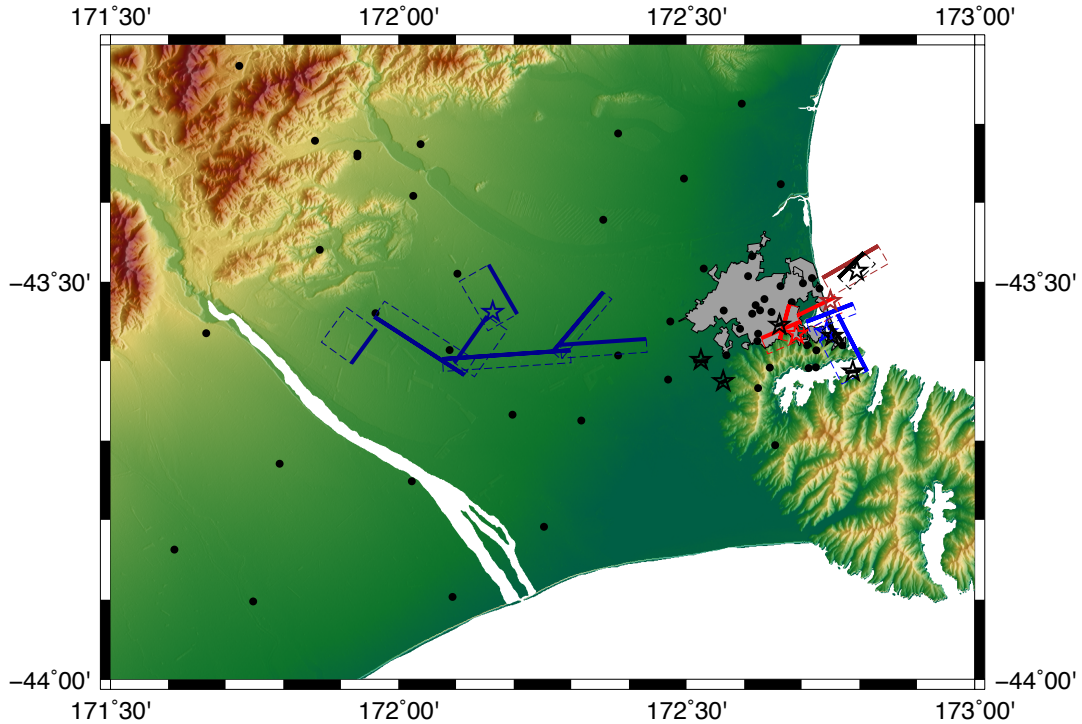

Figure 5: Illustration of 10 major events in the Canterbury earthquake sequence (the four largest shown as finite faults, the remaining six as point sources with epicentres indicated by stars) and strong motion stations which recorded strong ground motions from these multiple events (modified from Bradley (2015)).

Figure 6 illustrates the between-event residuals as a function of vibration period for the 10 events considered, as well as the region-specific residual, $\delta L2L_l$. It can be seen that for short vibration periods ($T \sim < 0.3s$) the value of $\delta L2L_l$ is approximately zero, illustrating that the Bradley (2010) empirical model is, on average, unbiased for these short vibration periods, across the events and strong motion stations considered. However, as the vibration period increases the value of $\delta L2L_l$ increases, as already seen in Figure 3d and Figure 4d for the 4 September 2010 and 22 February 2011 events. Bradley (2012b) and Bradley and Cubrinovski (2011) have suggested that greater than predicted SA amplitudes at long periods in the 4 September 2010 and 22 February 2011 events, respectively, could be the result of: (i) near-source forward directivity; (ii) nonlinear response of soft surficial soils; (iii) basin-induced surface waves; and (iv) inherent model bias as a result of a limited amount of reliable ground motion records at long vibration periods. While all these points are plausible on a single ground motion observation by observation basis, the observations in Figure 6 are based on sites in the Canterbury region located at various azimuths from 10 different earthquake events. Firstly, forward directivity rupture effects would not systematically affect sites at the range of azimuths considered, and such effects would not be significant for smaller magnitude events. Secondly, as the majority of the stations considered are located on the Canterbury alluvial deposits, basin-induced surface waves and nonlinear response of surficial soils are likely of importance, since only ground motions from moderate-to-large magnitude earthquakes at close distances were considered (i.e. the average PGA of the considered motions is 0.183g). Finally, while inherent model bias is a possibility for very long periods (i.e. $T > 5s$), it is unlikely at shorter periods (i.e. T=1s), and therefore this is not considered as a significant factor in the observed departure from zero in Figure 6.
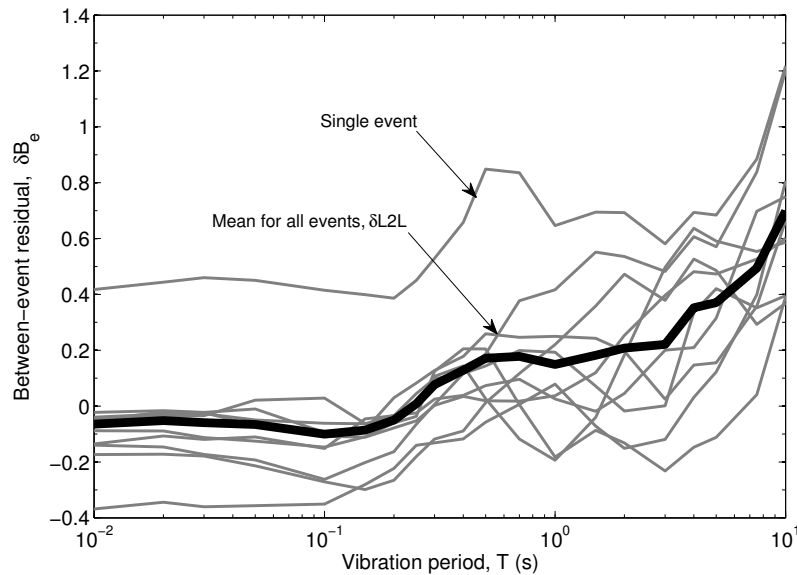

Figure 6: Ground motion between-event residuals for 10 major events in the Canterbury earthquake sequence, and the region-specific residual (bold line) (after Bradley (2015)).

Figure 7 illustrates two examples of the computation of the within-event residual, as well as the site-specific residual, $\delta S2S_s$. In Figure 7a it can be seen that the Christchurch Botanical Gardens (CBGS) station is relatively 'normal' in that its site-specific residual is relatively close to zero across the full range of vibration periods, although it is slightly above zero for T=0.4-4 seconds. In contrast, Figure 7b illustrates that the Heathcote Valley (HVSC) station has a site-specific residual which departs significantly from zero. This indicates that (relative to the prediction for a site class C site) the HVSC station ground motions exhibit systematically higher short period ($T \sim < 0.5s$) amplitudes, and systematically lower long period ($T \sim > 1s$) amplitudes.
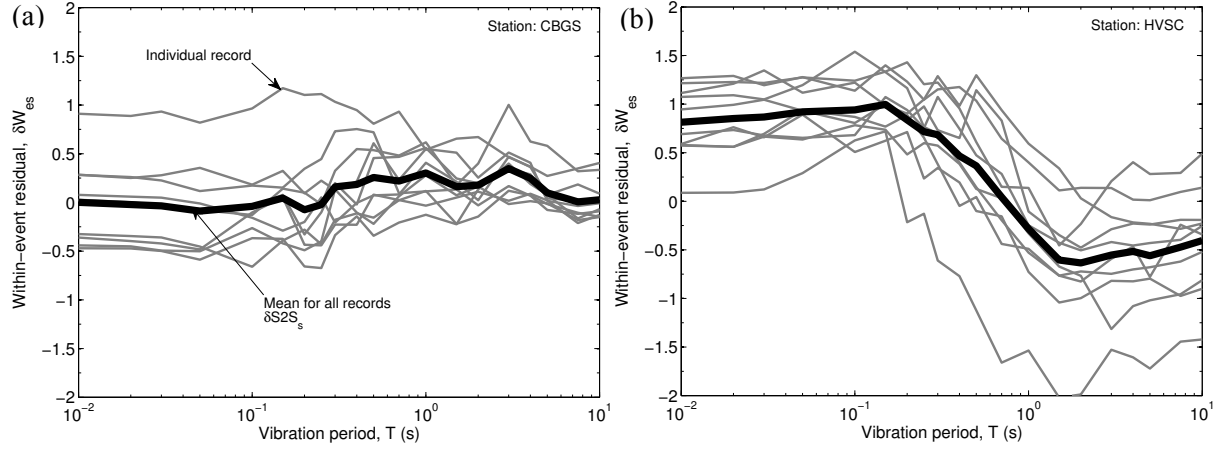
Figure 7: Examples of the within-event residuals at two strong motions stations (Christchurch Botanic Gardens, CBGS and Heathcote Valley, HVSC) for 10 major events, and the site-specific residuals (bold line). It can be seen that the CBGS station has a site-specific residual which is relatively close to zero, while the HVSC station site-specific residual departs from zero significantly (after Bradley (2015)).

On the basis that the region- and site-specific residuals ($\delta L2L_l$ and $\delta S2S_s$, respectively) are repeatable effects, they can be incorporated into the median prediction of a ground motion model to incorporate region- and site-specific effects. Figure 8 illustrates the implications of these repeatable effects in terms of the 'systematic amplification factor' which is applied to the median ground motion model. Firstly, the effect of the region-specific residual can be seen via all of the curves trending upwards as the vibration period increases. Secondly, it can be seen that there is significant variability in the systematic amplification factor across the different stations/suburbs. This important result clearly indicates that a significant portion of the total uncertainty in ground motion prediction results from the uncertainty in capturing the systematic response of each site (which is uncertain conditioned on the crude means of site classification via binary site class or V_{s30}). More detailed analyses of the observations in Figure 6-Figure 8 by Bradley (2015) demonstrates that approximately 40% of the total ground motion prediction uncertainty can be attributed to site-specific uncertainty, thus clearly illustrating the benefit of such empirical non-ergodic analysis (or the use of more fundamental physics-based approaches discussed subsequently) for appropriately capturing systematic effects and reducing uncertainty in prospective ground motion predictions.
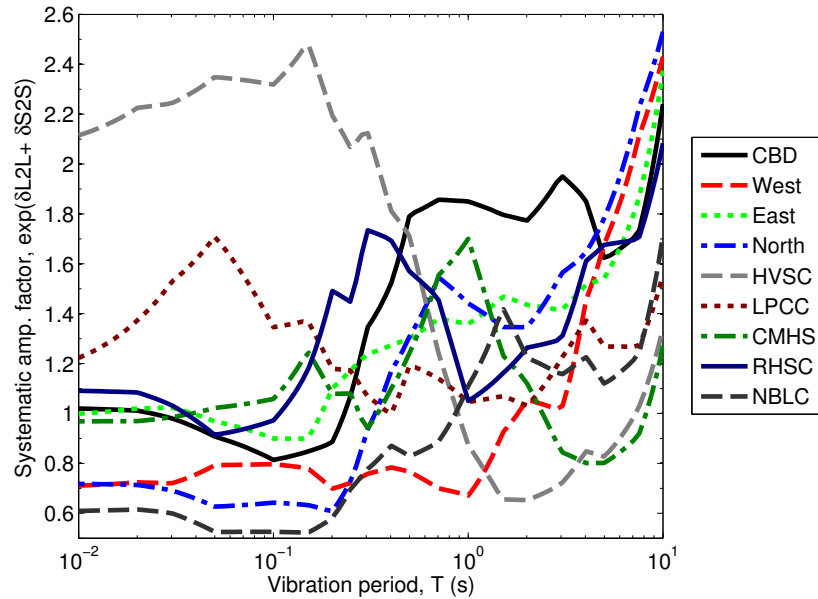

Figure 8: The effect of incorporation of region- and site-specific effects, as observed from non-ergodic ground motion analysis, in terms of the 'systematic amplification factor' applied to the ergodic median prediction. Stations are grouped into geographical regions, i.e. CBD and suburbs to the North, East, and West, with remaining stations that don't conform to a specific regional pattern being separately noted (after Bradley (2015)).

4 PREDICTIONS FROM PHYSICS-BASED MODELS

The previous section examined comparisons of the observed ground motions in the Canterbury earthquakes with empirical ground motion models. It was seen that generally speaking, the observed strong motions were consistent with empirical models, although there was notable variability in the responses, as well as some systematic biases. The biases were examined via non-ergodic empirical analysis leading to empirical systematic amplification factors for use in prospective predictions. The limitations of non-ergodic analysis from empirical models is that it requires sufficient high-amplitude ground motion observations at the site of interest (or the tenuous leap from systematic observations at small amplitude to the large amplitudes of engineering interest), and also that there is not a direct causative link between observed systematic effects and their underlying salient physical phenomena. The use of physics-based models offer a means to obtain ground motion predictions which contain more realistic region- and site-specific features (not without pitfalls however). This section examines the use of physics-based models for site-specific near-surface response analysis at Heathcote Valley and also hybrid broadband simulation and the pros and cons they offer over the use of empirical models, as discussed in the previous section.

4.1 *Site response simulations at Heathcote Valley*

As already alluded to with respect to the result of Figure 7b, the Heathcote Valley strong motion station recorded ground motions with short period amplitudes that were consistently larger than that predicted by empirical models for a shallow soil site. For comparison, Figure 9 illustrates the horizontal and vertical ground motions recorded at HVSC during the three largest amplitude strong motions, as well as those recorded at the nearby LPCC station (3km away). It can be seen that for all these events, the HVSC station has significantly higher horizontal and vertical acceleration amplitudes. Further empirical analysis of the HVSC records can be found elsewhere (Bradley 2012b, Bradley and Baker 2015, Bradley and Cubrinovski 2011).
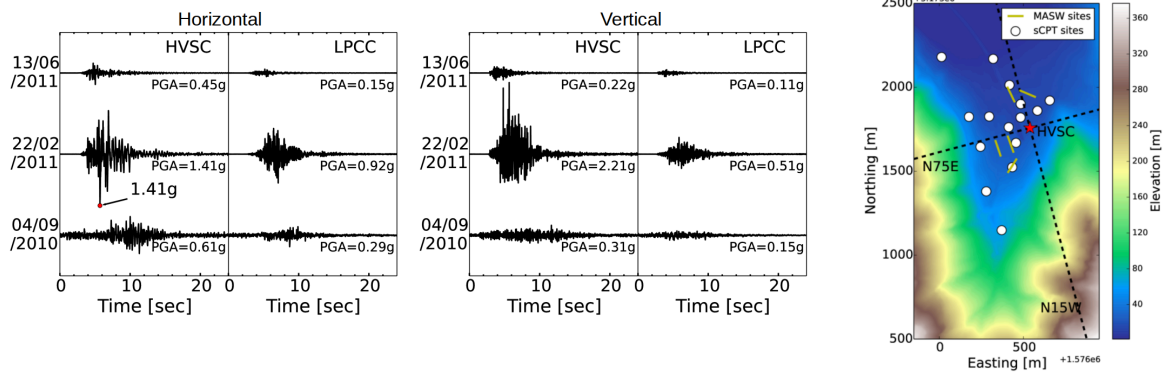

Figure 9: Comparison of horizontal and vertical ground motion acceleration times series recorded at Heathcote Valley (HVSC) and Lyttelton Port (LPCC) during the three strongest earthquake events and site characterisation in Heathcote Valley (after Jeong and Bradley (2015)).

The HVSC strong motion station is located near the head of the Heathcote Valley, in which shallow colluvium overlies rock from the Banks Peninsula volcanics. As a result, Bradley (2012b) hypothesised that the observed HVSC strong motions were significantly affected by the generation of basin-diffracted surface waves. In order to examine in further detail the salient phenomena resulting in the HVSC motions, a significant effort was undertaken to characterise the near-surface soil characteristics in the valley through sCPT, seismic refraction, and MASW analyses as shown in Figure 9 (Jeong et al. 2014). Subsequently, a series of 1D and 2D analyses have been completed of the valley response (with 3D analyses ongoing). Figure 10 illustrates the finite element geometries of the modelled valley in two orthogonal directions. It can be seen that the models account for both the topography of the free surface, as well as the inclined geometry of the colluvium-rock interface below the valley surface. The simulations were performed in OpenSees (McKenna et al. 2004), in which the colluvium is modelled as a pressure-dependent multi-yield (PDMY) constitutive model (Yang et al. 2003) and the volcanics as visco-elastic. Further modelling details can be found in Jeong and Bradley (2015).
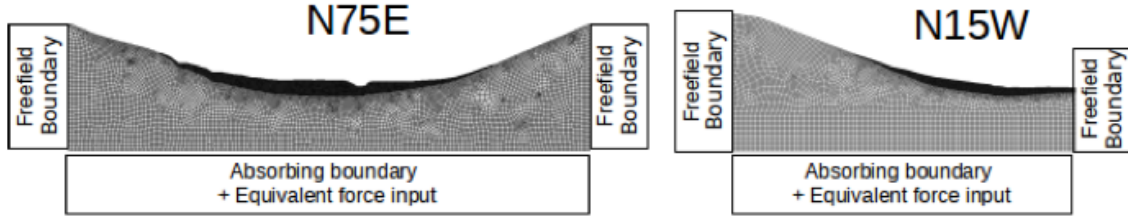
8

Figure 10: Finite element mesh geometries in two orthogonal directions (azimuth 75 and 345 degrees, respectively) used for 2D numerical simulations (after Jeong and Bradley (2015)).

Figure 11 provides a comparison of the simulated and observed response spectra at the location of the HVSC station for the 4 September 2010 and 22 February 2011 earthquakes. The response spectra of the input motion used in the simulations is also shown, which was based on deconvolution of the nearby LPCC motion, which was then amplitude scaled by the ratio of the source-to-site distances of the LPCC and HVSC stations for each specific event. It can be seen that for both events the observed and simulated responses exhibit a similar spectral shape, albiet with small-scale deviations.

To put the results for the 4 September 2010 and 22 February 2011 earthquakes in perspective, Figure 12 illustrates the residuals (i.e. $z = \ln{(obs/sim)}$) of the response spectral amplitudes as a function of vibration period for 9 events considered by Jeong and Bradley (2015). While there is clearly variability in the residual values as a function of period, it can be seen that the mean residual from these nine different simulations is relatively independent of vibration period. This is in contrast to the significant variation in the comparable mean residual from the empirical analysis shown in Figure 7b. The average value of the mean residual over all periods is 0.18, which corresponds to an average under-prediction of $\exp(0.18) = 1.2$. The reason for this under-prediction requires further investigation, but is within the error bounds of the assumed rock shear wave velocities at the depth of the input motion and the effects of anelastic attenuation. In summary, the significantly reduced bias of the mean residual shown in Figure 12, relative to that in Figure 7b, underlines the additional value gained by the use of site-specific near-surface response analysis as opposed to simplified site response prediction via empirical ground motion modelling.
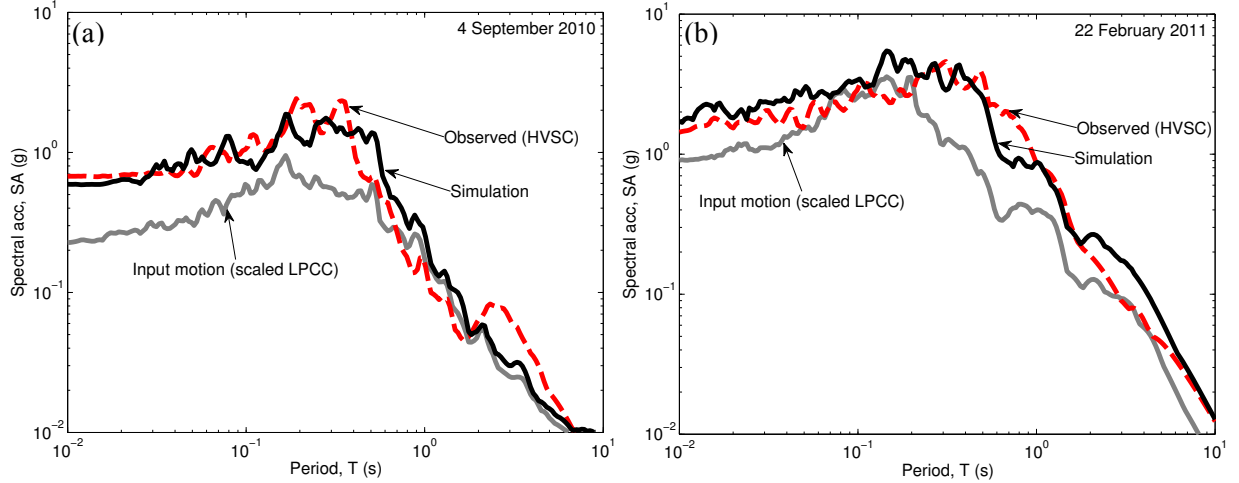

Figure 11: Comparison of simulated and observed ground motion response spectra at the HVSC station location, (azimuth 75 degrees) from the finite element model in Figure 10a, for the: (a) 4 September 2010; and (b) 22 February 2011 earthquakes.
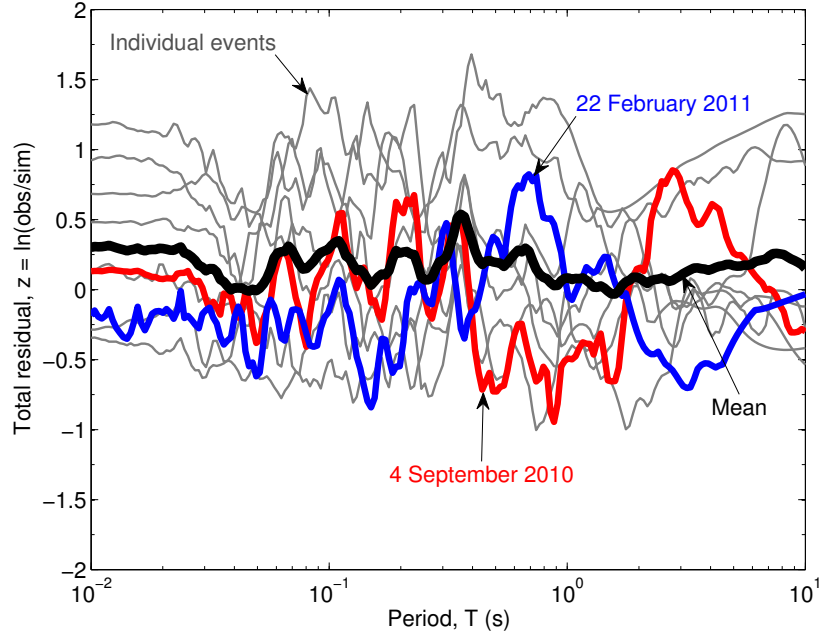
Figure 12: Residuals ($z = \ln(obs/sim)$) in predicting response spectral amplitudes at the Heathcote Valley strong motion station (HVSC) for 9 events considered by Jeong and Bradley (2015).

4.2 *Hybrid broadband simulations of the Canterbury earthquakes*

Ground motion simulation based on a physical representation of the seismic source, a 3D model of the geophysical properties of the earth's crust, and site-specific near-surface soil stratigraphy can provide significant physical insight into salient ground motion phenomena beyond that obtainable from a comparison of observations with empirical ground motion models. In this section, a summary of hybrid broadband ground motion simulation results based on the method of Graves and Pitarka (2015, 2010) is presented.

Ground motion simulation was performed for the 10 events noted in Figure 5. The largest four events (4/09/2010, 22/2/2011, 13/06/2011, 23/12/2011) were modelled as kinematic finite faults, while the six smaller events are considered as point sources. The finite fault models are based on the source inversion geometries of Beavan et al. (2011, 2012, 2010). Three of these four 'main' earthquakes in the sequence are postulated to have occurred on multiple fault planes. For simplicity, only the 4 September 2010 Darfield earthquake is modelled with multiple fault planes, and the single fault geometries for the 22 February and 13 June earthquakes are considered. The source geometry and hypocentre of Beavan et al. are utilized, but the slip distribution is stochastic following Graves and Pitarka (2015, 2010).

The 3D representation of the shallow crust in the Canterbury region utilizes version 1.61 of the Canterbury Velocity Model (CantVM) (Bradley et al. 2015, Lee et al. 2015). This model utilizes data from travel time tomography, seismic reflection, petroleum and hydrologic wells, active and passive surface wave analysis, and seismic CPT. The model provides a detailed representation of the surface of the Torlesse basement rock and Banks Peninsula volcanics, which are the two large impedance surfaces which have a strong influence on seismic wave propagation in the region.

The Graves and Pitarka simulation method utilizes a hybrid approach in which ground motion at low frequencies is obtained from 3D wave propagation, and stochastic simulation at high frequencies. The low frequency simulation ($f \leq 1$Hz) solves the viscoelastic wave propagation problem using a kinematic representation of the rupture source and 3D heterogenous crustal structure based on a staggered-grid finite difference scheme with 4th and 2nd order accuracy in space and time. Anelastic attenuation is considered as a function of shear wave velocity: $Q_p = 100V_s; Q_s = 50V_s$. A minimum shear wave velocity of 500m/s; and a spatial grid spacing of 0.1km are utilized to enable an accurate simulation of frequencies up to f=1Hz. The high-frequency simulation ($f \geq 1$Hz) is based on a semi-empirical stochastic approach in a 1D velocity structure for the region (Bradley and Graves 2014) in

which the following parameters were adopted: stress drop, $\Delta\sigma$=4MPa; Anelastic attenuation, $Q = Q_o f^x$, where $Q_0 = 41 + 34V_s$ and $x = 0.6$; and high frequency attenuation, κ=0.045. In the presented results, local site effects are incorpated via the simplified empirical approach of Campbell and Bozorgnia (2008) as discussed in Graves and Pitarka (2010), although we are presently working to couple these broadband ground motion simulations with site-specific near-surface site response (such as that discussed in the previous section).

Figure 13 and Figure 14 provide illustrations of the simulated ground velocities during the 4 September 2010 Darfield and 22 February 2011 Christchurch earthquakes, respectively. In the 4 September 2010 event, the four images at time increments of 5 seconds clearly illustrate: the significant forward directivity effects that develop at the eastern and western edges of the rupturing faults (t=16s); the modification of the eastward propagating directivity pulse as it encounters the Banks Peninsula volcanic region leading to focusing to the North in Christchuch (t=21s); and the significant basin-induced surface waves which propagate through Christchurch city to the east, and bounded by the significant basin edge caused by the Hororata fault to the west (t=26 and 31s). The significance of directivity and basin-generated surface waves are also prominent in the 22 February 2011 event, but have notably different effects on the observed ground motion intensity in which Figure 14 illustrates: the significant rupture directivity near the surface projection of the fault resulting from the up-dip rupture of this reverse oblique rupture (t=5s); the significant amplitudes produced from coupling of the directivity effect with the sedimentary basin to the North in Christchurch as compared to the amplitudes seen to the South across Banks Peninsula (t=8s); and the significant surface waves which dominate the later half of the ground motion (t=11 and 15s).
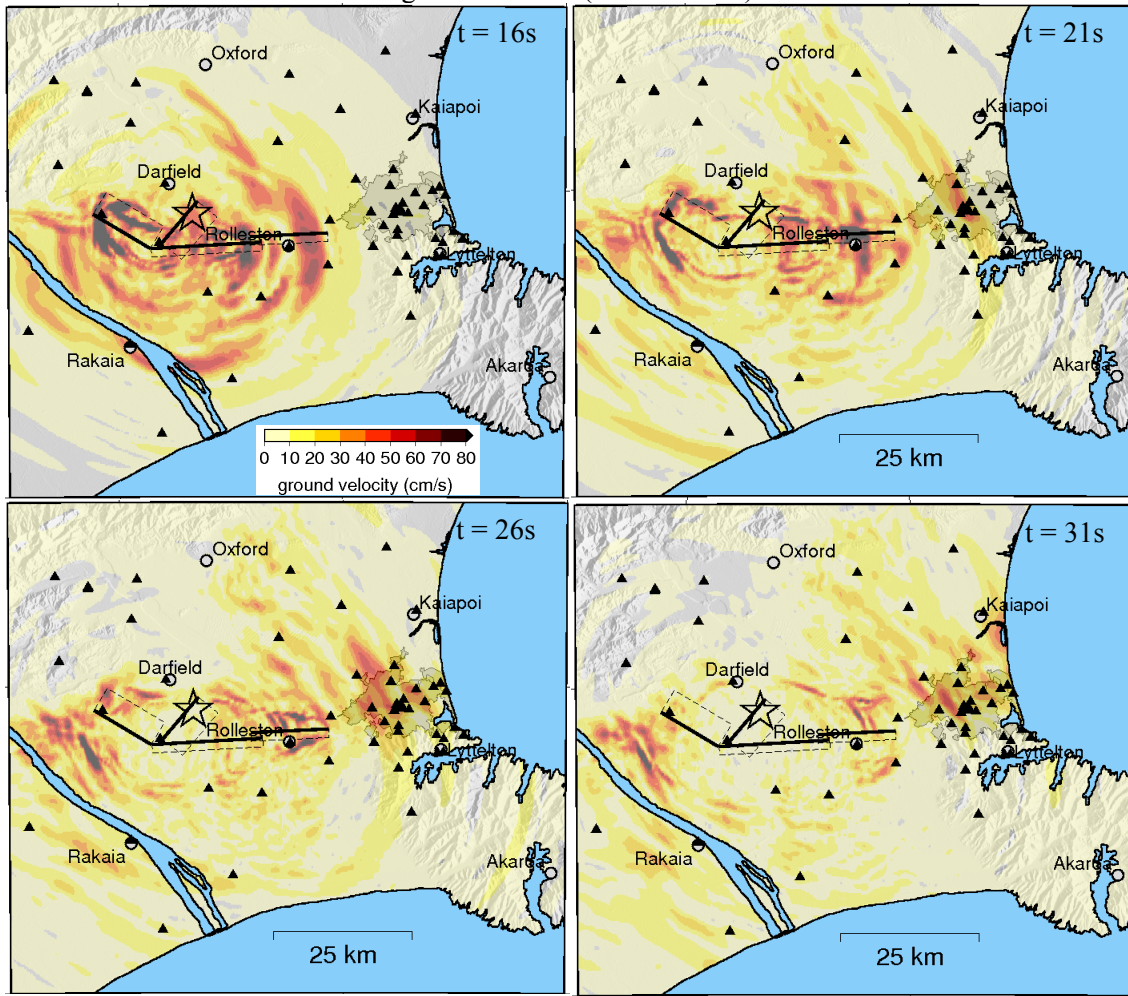

Figure 13: Simulation of the velocity wavefield at four time instants during the 4 September 2010 Darfield earthquake. Forward directivity effects toward Christchurch and basin-generated surface waves through the city toward Pegasus Bay and at the edge of the Hororata fault to the west are particularly pronounced.
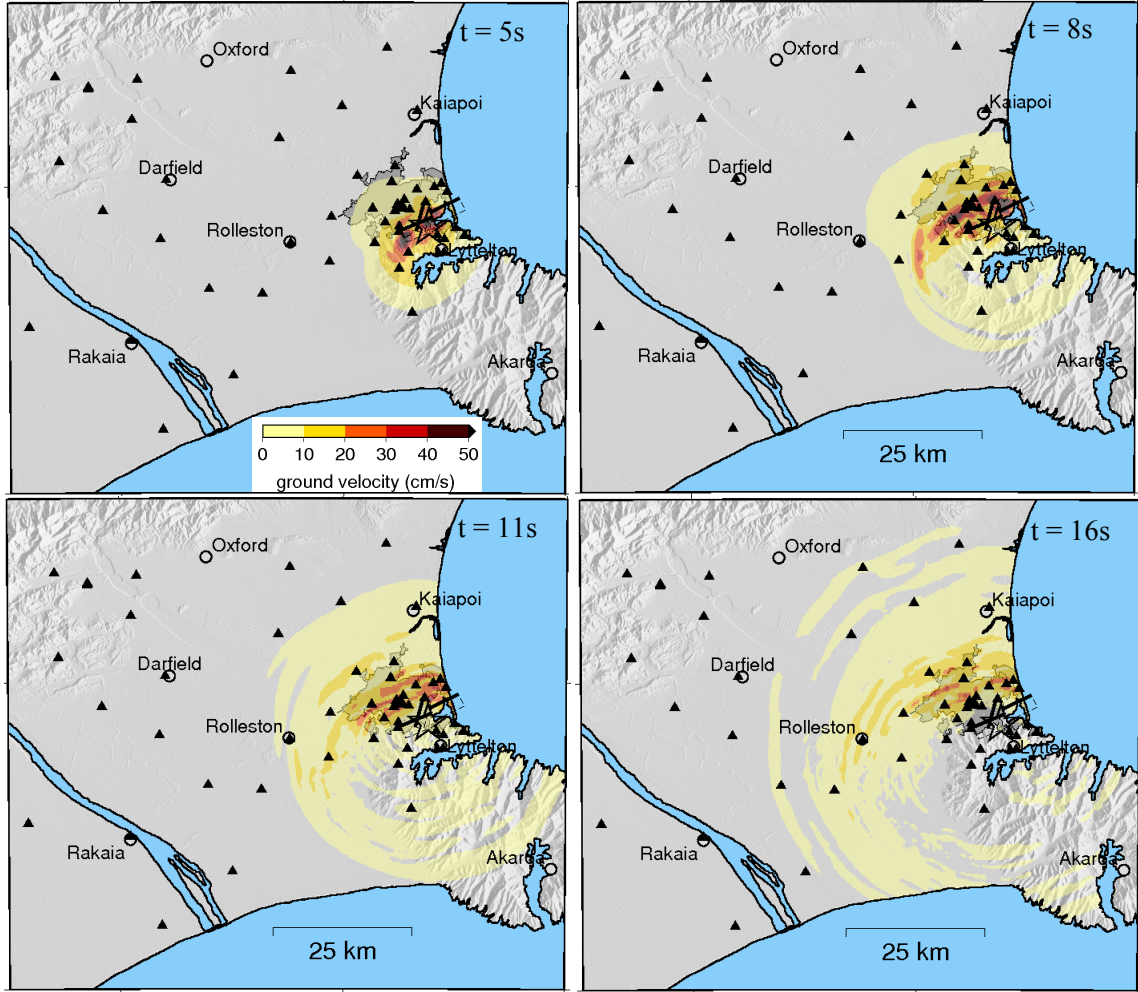
Figure 14: Simulation of the velocity wavefield at four time instants during the 22 February 2011 Christchurch earthquake. The directivity-basin coupling leads to significantly greater motions in the city to the north of the fault than those at similar distances in other directions.

Figure 15 provides a quantitative validation of the simulated ground motion intensity for the illustrations in Figure 13 and Figure 14, in which the observed, simulated, and empirically predicted long-period spectral ordinates are compared for *T*=1, 3, and 10 seconds (long periods are focused on because of the poor performance of the empirical models at such periods, as shown in Figure 6). It can be seen that the correlation between the observations and simulations is best at *T*=10s in which the simulations clearly capture the amplitude-variability for a given distance seen in the observations, and amplitudes that are, on average, larger than the median empirical prediction. It can also been seen in the *T*=3s ordinates that the simulations capture the large observed ground motion amplitudes in Christchurch (for which R_{rup}=15-20km and 2-8km in the Darfield and Christchurch events, respectively) resulting from directivity-basin coupling. The slight systematic over-prediction of the simulations for *T*=1 and 3 seconds is postulated as a result of neglecting a weathered layer in the current representation of the Banks Peninsula volcanics in the v1.61 CantVM velocity model utilized – which is being currently explored.
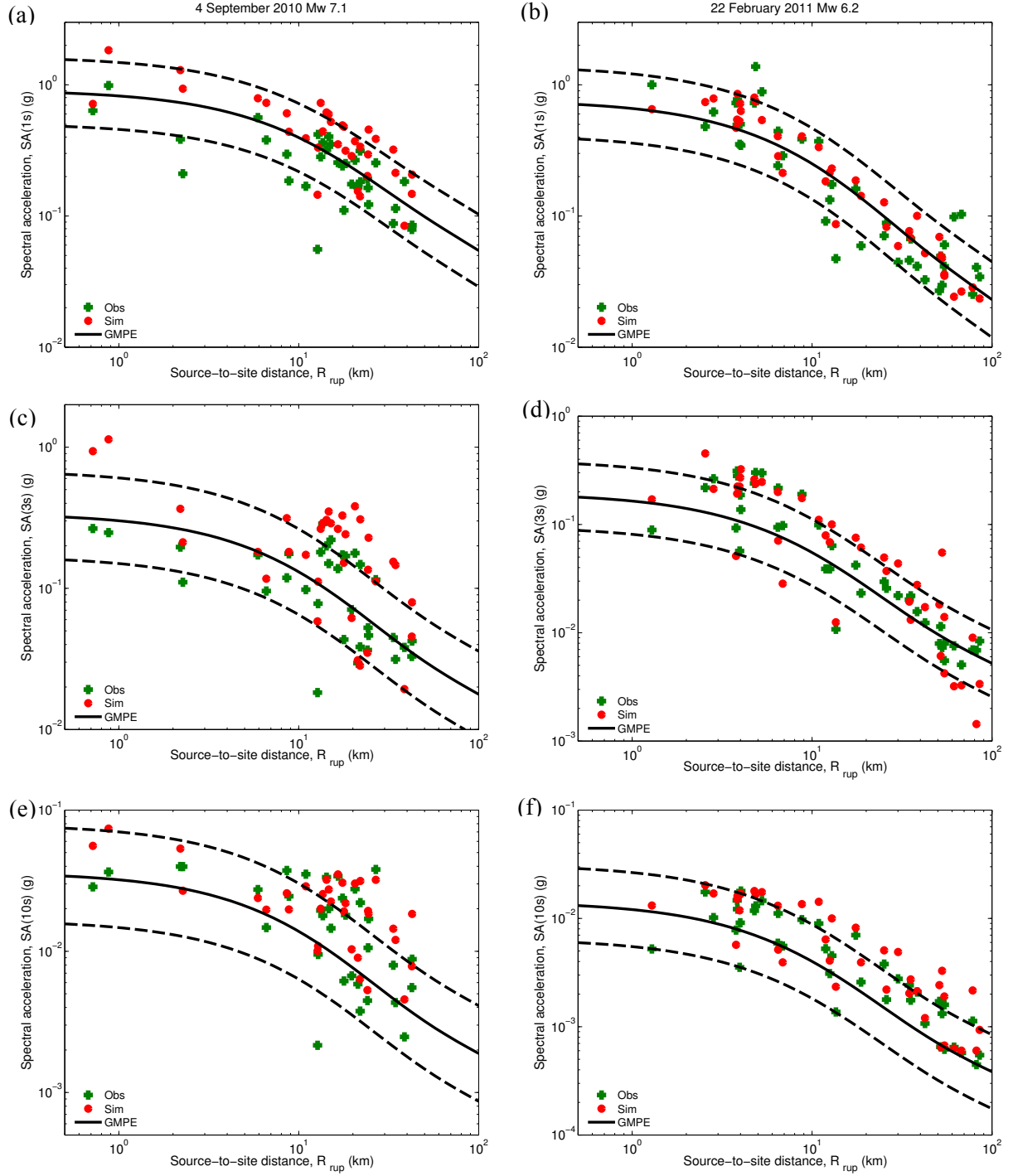
Figure 15: Comparison of long-period (T=1, 3, 10s) pseudo-acceleration response spectral amplitudes observed during the 4 September 2010 (left) and 22 February 2011 (right) earthquakes. Geometric mean observations and simulations at strong motion station locations are shown as points; as well as the median, 16th and 84th percentiles of the NZ-specific empirical model of Bradley (2013). Note that distances are as measured to the finite faults used in the simulations, which vary slightly from those used in the empirical results shown in Section 3.1.

Figure 16 provides a summary of the performance of the hybrid broadband ground motion simulation (based on the v1.61 CantVM velocity model) across the 10 considered earthquake events via the betwee-event residuals, i.e. the mean of ln (obs/sim) across all of the strong motion stations. It can be seen that for 7 of the 10 events, the simulations generally over-predict the observed spectral amplitudes for periods in the range of T=1-5s, which is inferred as a result of an excessive impedance contrast to the Banks Peninsula volcanics (as noted previously). In contrast, for three of the 10 events

(13 June 2011, and two events on 23 December 2011) there is a general under-prediction of the observations, even at short vibration periods. The 13 June and 23 December Mw5.9 earthquakes are two of four events that are modelled as finite faults, and it is recognised that the quality of the adopted finite fault models is significantly less than the more well studied ruptures for the 4 September 2010 and 22 February 2011 earthquakes. Clearly further research is needed to resolve the apparent issues for these events (which are also present in comparisons with empirical predictions).
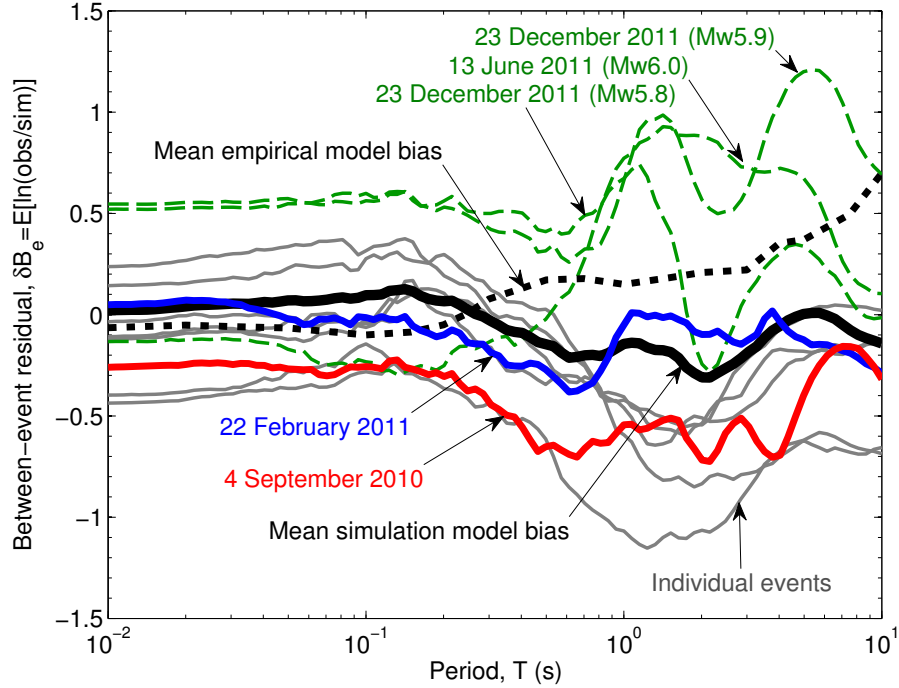

Figure 16: Between-event residuals from hybrid broadband ground motion simulation as a function of vibration period. The 4 September 2010 and 22 February 2011 are highlighted for comparison with previous results. The 13 June 2011, and two 23 December 2011 events are highlighted because of their significantly different predictions from observations, which is attributed to the relatively poor source representation for these offshore events, and the inferred multi-fault rupture of the 13 June 2011 event which is modelled as a single rupture plane in these results.

5 CONCLUSIONS

This paper has examined the predictive capabilities of empirical and physics-based ground motion models for 10 events in the 2010-2011 Canterbury earthquake sequence. The repeated recordings at the same set of locations in the observed strong motion dataset allowed insight into both the average performance of models across all strong motion stations, as well as any systematic biases at specific locations. The Heathcote Valley strong motion station (HVSC) was one such location in which observed response spectral amplitudes were seen to be systematically larger than observations at short periods ($T<1s$). The use of 2D numerical site response analyses at this location, to adequately capture the effect of the inclined basin edge, result in surface ground motion predictions which are consistent with the observed strong motion recordings. The use of physics-based hybrid broadband ground motion simulations provide significant physical insight into the salient forward directivity and basin-generated surface wave effects during the main events in the sequence, as well as quantitative predictions which rival those of the empirical methods. In summary, the comparison of both empirical and physics-based simulations against a set of 10 events in the Canterbury earthquake sequence clearly illustrates the potential for simulations to improve ground motion and site response prediction, both at present, and further in the future.

6 ACKNOWLEDGEMENTS

PhD students Robin Lee and Ethan Thomson provided significant input related to the Canterbury

REFERENCES:

Beavan J, Fielding E, Motagh M, Samsonov S and Donnelly N. 2011 Fault Location and Slip Distribution of the 22 February 2011 Mw 6.2 Christchurch, New Zealand, Earthquake from Geodetic Data. *Seismological Research Letters*; 82(6): 789-799.

Beavan J, Motagh M, Fielding EJ, Donnelly N and Collett D. 2012 Fault slip models of the 2010–2011 Canterbury, New Zealand, earthquakes from geodetic data and observations of postseismic ground deformation. *New Zealand Journal of Geology and Geophysics*; 55(3): 207-221.

Beavan J, Samsonov S, Motagh M, Wallace L, Ellis S and Palmer N. 2010 The Darfield (Canterbury) Earthquake: Geodetic observations and preliminary source model. *Bulletin of the New Zealand Society for Earthquake Engineering*; 43(4): 228-235.

Berrill JB, Avery H, Dewe M, Chanerley AA, Alexander NN, Dyer C, Holden C and Fry B. 2011 The Canterbury Accelerograph Network (CanNet) and some results from the September 2010, M7.1 Darfield Earthquake, in *9th Pacific Conference on Earthquake Engineering*: Auckland, New Zealand, 8.

Bradley BA. 2012a Ground motions observed in the Darfield and Christchurch earthquakes and the importance of local site response effects. *New Zealand Journal of Geology and Geophysics*; 55(3): 279-286.

Bradley BA. 2012b Strong ground motion characteristics observed in the 4 September 2010 Darfield, New Zealand earthquake. *Soil Dynamics and Earthquake Engineering*; 42 32-46.

Bradley BA. 2013 A New Zealand-Specific Pseudospectral Acceleration Ground-Motion Prediction Equation for Active Shallow Crustal Earthquakes Based on Foreign Models. *Bulletin of the Seismological Society of America*; 103(3): 1801-1822.

Bradley BA. 2015 Systematic ground motion observations in the Canterbury earthquakes and region-specific non-ergodic empirical ground motion modeling. *Earthquake Spectra*; (in press).

Bradley BA and Baker JW. 2015 Ground motion directionality in the 2010–2011 Canterbury earthquakes. *Earthquake Engineering & Structural Dynamics*; 44(3): 371-384.

Bradley BA and Cubrinovski M. 2011 Near-source Strong Ground Motions Observed in the 22 February 2011 Christchurch Earthquake. *Seismological Research Letters*; 82(6): 853-865.

Bradley BA and Graves RW. 2014 Low frequency (f≤1Hz) ground motion simulations of 10 events in the 2010-2011 Canterbury earthquake sequence, in *Southern California Earthquake Centre (SCEC) Annual Meeting*: Palm Springs, California.

Bradley BA, Lee RL, Thomson EM, Ghisetti F, McGann C, Pettinga JR and Hughes MW. 2015 3D Canterbury Velocity Model (CantVM) - Version 1.0, in *Southern California Earthquake Center (SCEC) Annual Meeting*: Palm Springs, CA.

Bradley BA, Quigley MC, Van Dissen RJ and Litchfield NJ. 2014 Ground Motion and Seismic Source Aspects of the Canterbury Earthquake Sequence. *Earthquake Spectra*; 30(1): 1-15.

Bray J, Cubrinovski M, Zupan J and Taylor M. 2014 Liquefaction Effects on Buildings in the Central Business District of Christchurch. *Earthquake Spectra*; 30(1): 85-109.

Buchanan A, Carradine D, Beattie GJ and Morris H. 2011 Performance of houses during the Christchurch earthquake of 22 February 2011. *Bulletin of the New Zealand Society for Earthquake Engineering*; 44(4): 342-357.

Campbell KW and Bozorgnia Y. 2008 NGA Ground Motion Model for the Geometric Mean Horizontal Component of PGA, PGV, PGD and 5% Damped Linear Elastic Response Spectra for Periods Ranging from 0.01 to 10 s. *Earthquake Spectra*; 24(1): 139-171.

Clifton C, Bruneau M, MacRae GA, Leon RT and Fussell A. 2011 Steel Structures Damage from the Christchurch Earthquake Series of 2010 and 2011. *Bulletin of the New Zealand Society for Earthquake Engineering*; 44(4): 297-318.

Cubrinovski M, Bradley BA, Wotherspoon L, Green AG, Bray J, Wood C, Pender M, Allen CR, Bradshaw A, Rix G, Taylor M, Robinson K, Henderson D, Giorgini S, Ma K, Winkley A, Zupan J, O'Rourke TD, DePascale G and Wells DL. 2011a Geotechnical Aspects of the 22 February 2011 Christchurch Earthquake. *Bulletin of the New Zealand Society for Earthquake Engineering*; 44(4): 205-226.

Cubrinovski M, Bray JD, Taylor M, Giorgini S, Bradley B, Wotherspoon L and Zupan J. 2011b Soil Liquefaction Effects in the Central Business District during the February 2011 Christchurch Earthquake. *Seismological Research Letters*; 82(6): 893-904.

Dellow G, Yetton M, Massey C, Archibald G, Barrell D, Bell D, Bruce Z, Campbell A, Davies T, De Pascale GP, Easton M, Forsyth PJ, Gibbons C, Glassey P, Grant H, R. G, Hancox G, Jongens R, Kingsbury P, Kupec J, Macfarlane D, McDowell B, McKelvey B, McCahon I, McPherson I, Molloy J, Muirson J, O'Halloran M, Perrin N, Price C, Read S, Traylen NJ, Van Dissen R, Villeneuve M and Walsh I. 2011 Landslides caused by the 22 February 2011 Christchurch earthquake and management of landslide risk in the immediate aftermath. *Bulletin of the New Zealand Society for Earthquake Engineering*; 44(4): 227-238.

Gledhill K, Ristau J, Reyners M, Fry B and Holden C. 2011 The Darfield (Canterbury, New Zealand) Mw 7.1 Earthquake of September 2010: A Preliminary Seismological Report. *Seismological Research Letters*; 82(3): 378-386.

Graves R and Pitarka A. 2015 Refinements to the Graves and Pitarka (2010) Broadband Ground-Motion Simulation Method. *Seismological Research Letters*; 86(1): 75-80.

Graves RW and Pitarka A. 2010 Broadband Ground-Motion Simulation Using a Hybrid Approach. *Bulletin of the Seismological Society of America*; 100(5A): 2095-2123.

Jeong S and Bradley BA. 2015 Simulation of 2D site response at Heathcote Valley during the 2010-2011 Canterbury earthquake sequence, in *10th Pacific Conference on Earthquake Engineering*: Sydney, Australia, 8.

Jeong S, Bradley BA, McGann CR and DePascale G. 2014 Characterization of dynamic soil properties and stratigraphy at Heathcote Valley, New Zealand, for simulation of 3D valley effects, in *Southern California Earthquake Centre (SCEC) Annual Meeting*: Palm Springs, California.

Kaiser A, Holden C, Beavan J, Beetham D, Benites R, Celentano A, Collett D, Cousins J, Cubrinovski M, Dellow G, Denys P, Fielding E, Fry B, Gerstenberger M, Langridge R, Massey C, Motagh M, Pondard N, McVerry G, Ristau J, Stirling M, Thomas J, Uma SR and Zhao J. 2012 The Mw 6.2 Christchurch earthquake of February 2011: preliminary report. *New Zealand Journal of Geology and Geophysics*; 55(1): 67-90.

Kam WY, Pampanin S and Elwood KJ. 2011 Seismic performance of reinforced concrete buidlings in the 22 Febraury Christchurch (Lyttelton) Earthquake. *Bulletin of the New Zealand Society for Earthquake Engineering*; 44(4): 239-278.

Lee RL, Bradley BA, Ghisetti F, Thomson EM, Pettinga JR and Hughes MW. 2015 A geology-based 3D seismic velocity model of Canterbury, New Zealand, in *New Zealand Society for Earthquake Engineering (NZSEE) Annual Conference*: Rotorua, 8.

Marquis F, Kim J, Elwood KJ and Chang SE. 2015 Post-earthquake decisions: A case-study of multi-storey concrete buildings in Christchurch, in *New Zealand Society for Earthquake Engineering Annual Conference*: Rotorua, New Zealand, 12.

Massey CI, McSaveney MJ, Taig T, Richards L, Litchfield NJ, Rhoades DA, McVerry GH, Lukovic B, Heron DW, Ries W and Van Dissen RJ. 2014 Determining Rockfall Risk in Christchurch Using Rockfalls Triggered by the 2010–2011 Canterbury Earthquake Sequence. *Earthquake Spectra*; 30(1): 155-181.

McKenna F, Fenves GL and Scott MH. 2004 OpenSees: Open system for earthquake engineering simulation. Pacific Earthquake Engineering Research Center, University of California, Berkeley, CA.

Quigley MC, Bastin S and Bradley BA. 2013 Recurrent liquefaction in Christchurch, New Zealand, during the Canterbury earthquake sequence. *Geology*; 41(4): 419-422.

Yang Z, Elgamal AW and Parra E. 2003 Computational model for cyclic mobility and associated shear deformation. *Journal of Geotechnical and Geoenvironmental Engineering*; 129(12): 1119-1127.